Stem Cell Reports
Article

The Long Noncoding RNA *Lncenc1* Maintains Naive States of Mouse ESCs by Promoting the Glycolysis Pathway

Zihao Sun,[1,5] Minzhe Zhu,[1,5] Pin Lv,[1,5] Lu Cheng,[1,5] Qianfeng Wang,[1] Pengxiang Tian,[1] Zixiang Yan,[1] and Bo Wen[2,3,4,*]

[1]MOE Key Laboratory of Metabolism and Molecular Medicine, School of Basic Medical Sciences, Institutes of Biomedical Sciences, Fudan University, Shanghai 200032, China
[2]The Fifth People's Hospital of Shanghai, Institutes of Biomedical Sciences, Fudan University, Shanghai 200032, China
[3]MOE Key Laboratory of Metabolism and Molecular Medicine, Department of Biochemistry and Molecular Biology, School of Basic Medical Sciences, Fudan University, Shanghai 200032, China
[4]State Key Laboratory of Genetic Engineering, Collaborative Innovation Center of Genetics and Development, Fudan University, Shanghai 200438, China
[5]Co-first author
*Correspondence: bowen75@fudan.edu.cn
https://doi.org/10.1016/j.stemcr.2018.08.001

SUMMARY

The naive embryonic stem cells (nESCs) display unique characteristics compared with the primed counterparts, but the underlying molecular mechanisms remain elusive. Here we investigate the functional roles of *Lncenc1*, a highly abundant long noncoding RNA in nESCs. Knockdown or knockout of *Lncenc1* in mouse nESCs leads to a significantly decreased expression of core pluripotency genes and a significant reduction of colony formation capability. Furthermore, upon the depletion of *Lncenc1*, the expression of glycolysis-associated genes is significantly reduced, and the glycolytic activity is substantially impaired, as indicated by a more than 50% reduction in levels of glucose consumption, lactate production, and extracellular acidification rate. Mechanistically, *Lncenc1* interacts with PTBP1 and HNRNPK, which regulate the transcription of glycolytic genes, thereby maintaining the self-renewal of nESCs. Our results demonstrate the functions of *Lncenc1* in linking energy metabolism and naive state of ESCs, which may enhance our understanding of the molecular basis underlying naive pluripotency.

INTRODUCTION

Pluripotent stem cells (PSCs) can self-renew indefinitely and harbor the capability to generate almost all cells of an organism, thus holding a great promise in medical applications (De Los Angeles et al., 2015; Martello and Smith, 2014). Mouse embryonic stem cells (ESCs), the first derived PSCs, were obtained from the inner cell mass of the blastocyst (Evans and Kaufman, 1981; Martin, 1981). Epiblast stem cells (EpiSCs), a newer type of PSCs, were derived from the post-implantation embryo of the mouse (Brons et al., 2007; Tesar et al., 2007). It was proposed that ESCs and EpiSCs represent two different states of pluripotency: the naive and primed state, corresponding to pre- and post-implantation epiblasts *in vivo*, respectively (Marks et al., 2012). ESCs cultured in conventional serum/feeder systems are heterogonous cells with multiple pluripotent states. By contrast, ESCs cultured in 2i/LIF, i.e., ground-state ESCs or naive ESCs (nESCs), are relatively homogeneous. The nESCs harbor unique characteristics including high capability of colony formation, expression of naive pluripotency genes, global DNA hypomethylation, reactivation of two X chromosomes in female cells, and uses of both glycolysis and oxidative metabolism, mostly reflecting naive pluripotency *in vivo* (Hackett and Surani, 2014). Furthermore, nESCs can be converted into epiblast-like cells (EpiLCs) *in vitro* (Hayashi et al., 2011), representing

an intermediate state between nESCs and EpiSCs (Kalkan and Smith, 2014; Kurimoto et al., 2015).

The naive-state PSCs were initially derived in rodents including mouse (Li et al., 2008) and rat (Huang da et al., 2009). Recently, human naive-like PSCs were generated by overexpression of naive pluripotency factors (Takashima et al., 2014; Theunissen et al., 2014) or by isolating directly from early embryos (Guo et al., 2016). Human naive PSCs are similar to rodent PSCs on global transcriptional state, core transcription factor networks, and metabolism properties; however, there are still significant discrepancies regarding signaling profile and epigenetic identity (Bates and Silva, 2017), suggesting that our understanding of the molecular mechanisms of the naive state remains incomplete.

Long noncoding RNAs (lncRNAs), transcripts longer than 200 nucleotides without protein-coding capability, can regulate gene expression at transcriptional and post-transcriptional levels. They are emerging as important players in many biological processes including embryonic development, stem cell self-renewal, and differentiation (Flynn and Chang, 2014; Luo et al., 2016; Rosa and Ballarino, 2016). As one of the most commonly used cell models for lncRNA studies, PSCs have been extensively profiled for RNA expression, epigenetic modifications, and RNA-protein interactions (Guttman et al., 2009, 2011; Kelley and Rinn, 2012). Functional studies have indicated that

lncRNAs are involved in the self-renewal of PSCs through regulating key pluripotency factors (Kaneko et al., 2014; Perry and Ulitsky, 2016; Sheik Mohamed et al., 2010), mediating chromatin modifications (da Rocha et al., 2014; Jain et al., 2016; Lin et al., 2014), or sponging/counteracting microRNAs (Liu et al., 2017; Wang et al., 2013). However, the lists of potentially functional lncRNAs in ESCs that have been reported by different studies overlap poorly (Guttman et al., 2011; Kaneko et al., 2014), which suggests that the functions of lncRNAs in PSCs are still not yet fully understood. Here we profiled genome-wide lncRNA expressions in mouse nESCs and their derived EpiLCs, and investigated the functions of one of the highly expressed lncRNAs in nESCs.

RESULTS

The Profiling of lncRNAs in Mouse nESCs and EpiLCs

To investigate the transcripts of nESCs and EpiLCs, we performed strand-specific, ribosomal RNA-depleted RNA sequencing (RNA-seq) experiments in two independent mouse ESC lines (Figure 1A). Through differential expression (DE) analysis between nESCs and EpiLCs, 2,227 DE genes are detected (Figure 1B), including 2,025 mRNAs (1,196 upregulated and 829 downregulated) and 202 lncRNAs (67 upregulated and 135 downregulated). The full list of DE lncRNA genes is provided in Table S1.

To examine the functions of lncRNAs preferentially expressed in nESCs, we tested seven lncRNAs in the lists through small hairpin RNA (shRNA)-based RNAi. We selected these lncRNAs because they are relatively enriched in nESCs, and their functions remain unknown. We achieved a significant depletion of greater than 40% with both shRNAs targeting four of seven lncRNAs tested (*Lncenc1*, *Panct2*, *GM13110*, and *GM805*). Depletion of each of these lncRNAs was associated with a significant reduction in Oct4 and/or Nanog mRNA levels, along with visible flatting of clone morphologies, suggesting that these lncRNAs may play roles in maintaining the state of nESCs (Figure S1).

Lncenc1 Is Specifically Expressed in nESCs and Is Highly Dynamic during Differentiation

Among these lncRNAs, we decided to focus on *Lncenc1*, as (1) it is the most abundant lncRNA that is differentially expressed in nESCs (Table S1); (2) its gene locus overlaps a super-enhancer domain (Figure 1C), suggesting that it is potentially functional; and (3) it is specifically expressed in nESCs relative to somatic tissues (Figure 2A). We noticed a published mouse work, which knocked out a lncRNA named as *lincenc1* (Sauvageau et al., 2013), but the reported sequence transcribes from the opposite direction and does

not overlap with the *lncenc1* gene we studied here (Figure 1C).

To test the completeness of the *Lncenc1* transcript, we performed northern blot analysis. The data showed that the transcript is about 3,400 nucleotides in size in nESCs, but was almost undetectable in EpiLCs (Figure 2B). According to our RNA-seq data (Figure 1C) and RT-PCR analysis (Figure S2A), the shorter isoform (NR_110430) expresses in nESCs rather than the longer one (NR_110432). Furthermore, both RNA FISH and cellular fraction experiments indicated that transcripts of *Lncenc1* located in both the nucleus and cytoplasm of mouse nESCs (Figures 2C and 2D).

To study dynamic changes of *Lncenc1* expression during the nESC-to-EpiLC transition, we measured its expression over a 72-hr time window in E14 nESCs. The results showed that the expression level is relatively stable during the first 24 hr, but then decreases dramatically and becomes nearly undetectable after 72 hr (Figure 2E). Similar dynamics were observed in spontaneous differentiation induced by the withdrawal of 2i/LIF from the medium, and the decline of *Lncenc1* expression happened earlier at around hour 6 (Figure 2F). Interestingly, the decline of *Lncenc1* expression occurred after *Nanog* but before *Oct4* in both cases; this suggests that *Lncenc1* could be involved in pluripotency networks, consistent with a recent observation that the expression profile of *Lncenc1* is associated with known pluripotency genes (Bergmann et al., 2015). Similar expression dynamics were also observed in the R1 cell line (Figures S2B and S2C), indicating a general role of *Lncenc1* in nESCs. Functional experiments thereafter were performed only in E14 cells unless otherwise stated.

Lncenc1 Is Required for Self-Renewal in nESCs

To investigate the function of *Lncenc1*, we knocked down its expression in nESCs by two independent shRNAs, which can deplete 70%–80% of *Lncenc1* transcripts as shown by qRT-PCR. As a result, the expression of six pluripotency genes decreases significantly, although the magnitude of deduction is usually less than 50% (Figure 3A). Consistently, protein levels of OCT4, NANOG, and SOX2 are decreased in *Lncenc1* knockdown cells as shown by western blot and immunofluorescence (Figures S3A and S3B). Moreover, clone morphologies changed from "round and tight" to "flat and loose," and alkaline phosphatase staining became weaker in *Lncenc1*-knockdown cells (Figures 3B and S3C). As *Lncenc1* transcripts locate in both nucleus and cytosol, we also conducted antisense oligonucleotide (ASO)-mediated gene silencing, which showed higher knockdown efficiency compared with RNAi for nuclear RNAs (Lennox and Behlke, 2016). Consistently, when *Lncenc1* was suppressed by two independent ASOs, expression levels of core pluripotency genes were significantly decreased (Figure S3D).
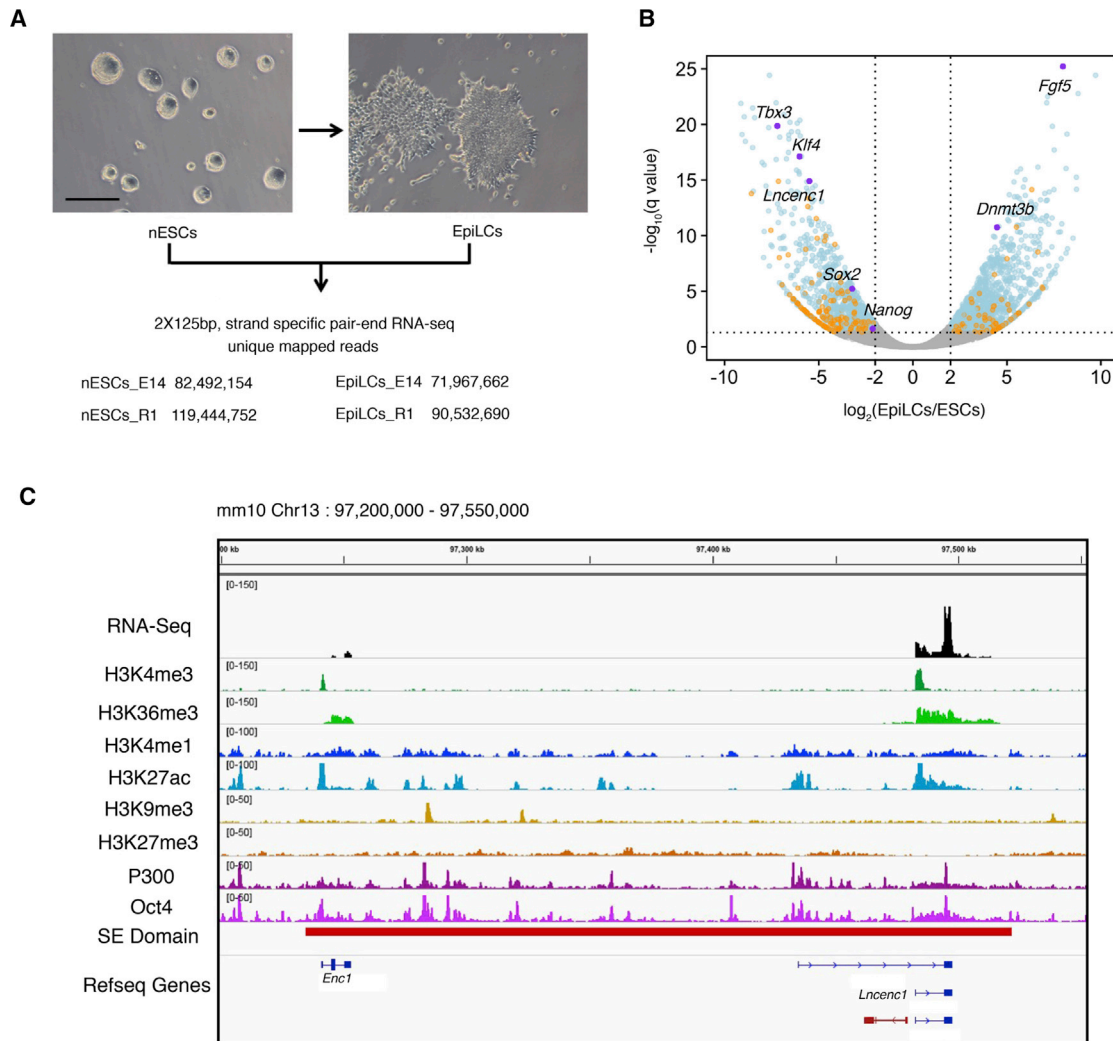
Figure 1. Profiling of Transcripts in nESC-to-EpiLC Transition

(A) Cell morphology changes during nESC-to-EpiLC transition and numbers of uniquely mapped reads from RNA-seq experiments conducted in two cell lines (E14 and R1).

(B) The volcano plot showing differentially expressed genes between nESCs and EpiLCs. Fold changes (log2) are plotted on the x axis, and q values ($-$log10 scale) are plotted on the y axis. Significantly changed genes (q < 0.05, log2 fold changes >2 or <$-$2) are indicated in blue (mRNAs) and orange (lncRNAs). Purple dots denote representative genes. See also Figure S1 and Table S1.

(C) Chromatin features in the *Lncenc1* locus. The top track shows normalized reads densities of RNA-seq results of nESCs. Tracks below show signals of histone modifications, TF binding, and the super-enhancer domain. P300, Oct4, H3K27ac, and H3K4me1 ChIP-seq data were from GEO: GSE56138; H3K4me3, H3K27me3, H3K36me3, and H3K9me3 ChIP-seq data were from GEO: GSE23943. Coordinates of super-enhancer domains were obtained from Dowen et al. (2014). The lncRNA named *lincenc1* (Sauvageau et al., 2013) is shown in red at the bottom track.

To further rule out potential off-target effects of shRNA- or ASO-based gene silencing, we generated *Lncenc1* knockout (KO) cell lines through CRISPR/Cas9-based genome editing technology. We successfully established four KO cell lines by deleting the entire gene locus or the largest exon, and *Lncenc1* transcripts were almost completely depleted in these cells. Compared with wild-type cells, the expression of pluripotency genes is significantly reduced in all these KO cell lines (Figure 3C). More important, colony formation capability, a proxy for self-renewal efficiency (Martello and Smith, 2014), was significantly decreased in knockdown and KO cells (Figure 3D).

To test whether *Lncenc1* is sufficient to maintain the naive state, we overexpressed *Lncenc1* (OE) in nESCs and
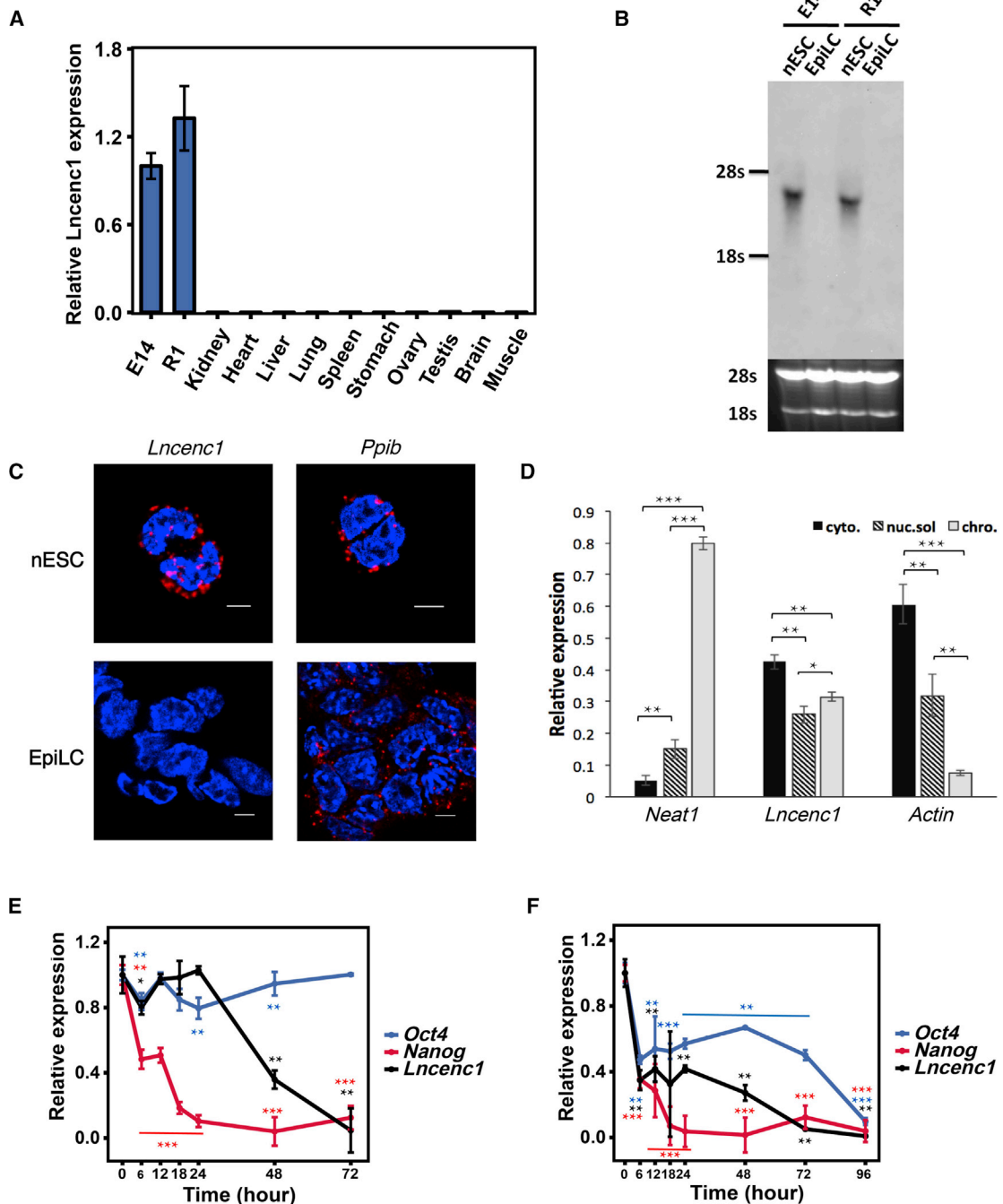
Figure 2. Characterization of *Lncenc1* and Its Expression Dynamics during ESC Differentiation

(A) Expression of *Lncenc1* in mouse nESCs and somatic tissues as measured by qRT-PCR. Expression levels were normalized against *Actb*. Results are shown as means ± SD of three independent experiments.

(B) The *Lncenc1* transcript detected by northern blot analysis. The agarose gel imaging (black background) underneath the blot (gray background) shows total RNA used for analysis.

(C) RNA *in situ* hybridization (RNAscope) targeting *Lncenc1* in mouse nESCs and EpiLCs. *Ppib* was used as a positive control. Nuclei were stained with DAPI. Scale bars, 5 μm.

(D) Relative expression levels of *Lncenc1* in cytoplasm, nucleoplasm, or chromatin fractions as determined by qRT-PCR analysis of RNA extracted from each fraction. *Neat1* and *Actb* were used as controls. Data are the means ± SD of three independent experiments. Statistical significance of t test: *p < 0.05, **p < 0.01, ***p < 0.001.

then withdrew 2i/LIF for 2 days. The morphology of OE cells is more "naive-like" compared with the control (Figure 3E). In the 2i/LIF culture (day 0), the expression levels of pluripotency genes tested are all significantly increased in the OE cells (Figure 3F). After the withdrawal of 2i/LIF for 1 day, the expression levels of pluripotency genes, especially naive-state genes (*Nanog*, *Tbx3*, *Rex1*, and *Esrrb*), remain significantly higher, whereas those of post-implantation genes (*Fgf5* and *Dnmt3b*) are significantly lower in the OE cells, suggesting that the overexpression of *Lncenc1* in nESCs delays their differentiation. On day 2, the expression levels of pluripotency genes decrease further and are comparable between OE and control cells. Therefore, *Lncenc1* is required but not sufficient to keep the ESCs in a naive state.

Lncenc1 Controls the Glycolysis Pathway in nESCs

To reveal global gene expression changes upon *Lncenc1* depletion, we conducted RNA-seq experiments with control and knockdown cells and identified 101 downregulated and 182 upregulated genes (Figure 4A; Table S2). Functional annotation of these affected genes indicated that they are highly enriched in the glycolysis/gluconeogenesis pathway (Figure 4B). We then examined mRNA expression with qRT-PCR in knockdown (by shRNAs and ASOs) and KO nESCs and confirmed that these glycolysis genes detected by RNA-seq are all significantly decreased upon depletion or deletion of *Lncenc1* (Figures 4C, 4D, and S3E). Consistently, protein levels of these glycolytic enzymes are markedly decreased in *Lncenc1* knockdown and KO cells as determined by western blotting (Figure 4E). Furthermore, upon the overexpression of *Lncenc1* in nESCs, the mRNA levels of glycolysis genes are upregulated significantly; however, after spontaneous differentiation, the control and OE ESCs display similar dynamic changes on these glycolysis genes (Figure 4F).

To test whether the functions of *Lncenc1* can be rescued in its depleted or deleted cells, we have re-expressed *Lncenc1* in the knockout and knockdown ESCs. Unfortunately, although *Lncenc1* can be re-expressed markedly, the expression of glycolysis and pluripotency genes still cannot be restored (Figure S4). These data suggest that increased expression alone might not be sufficient for *Lncenc1* activity. Other factors might also contribute toward making *Lncenc1* functional, such as the location of expression in the genome, and the localization of the ectopic *Lncenc1* RNAs.

Next, we examined the glycolytic activity through functional assays. First we measured the glucose consumption and lactate production, the "in and out" of glycolysis, and found that they are both significantly decreased in *Lncenc1* knockdown (Figure 5A) and KO (Figure 5B) cells compared with the controls. We further examined glycolytic activity through glycolysis stress tests. As expected, the level of glycolytic activity was significantly decreased in knockdown cells as indicated by the measurement of the extracellular acidification rate (ECAR), which is largely the result of glycolysis (Figure 5C). We measured the initial pH in glucose-free culture medium (non-glycolysis). Then, to activate glycolysis, we sequentially added oligomycin (a mitochondrial ATP synthase inhibitor) to the culture medium. Both before and after activation, the glycolytic rate of control cells was significantly higher than that of knockdown cells (Figure 5D). It is notable that, when knockdown experiments were conducted with sh*Lncenc1*-1, which displayed better efficiency, glucose consumption, lactate production, and ECAR were all reduced by 50% or more. These data indicate that the glycolysis activity was severely impaired after the downregulation of *Lncenc1*.

Lncenc1 Functionally Interacts with HNRNPK and PTBP1

To identify potential partners of *Lncenc1*, we performed the RNA pull-down assay using biotin-labeled probes. Compared with the antisense control, the pull-down sample with sense probe showed two specific bands on the SDS-PAGE gel, which were identified as PTBP1 and HNRNPK by mass spectrometry and further validated by western blotting (Figure 6A). Moreover, results of RNA immunoprecipitation against PTBP1 and HNRNPK antibodies showed that *Lncenc1* RNAs are highly enriched compared with the other six lncRNAs tested (Figure 6B), which further confirmed interactions between *Lncenc1* and these two proteins. The yeast two-hybrid assay showed that PTBP1 and HNRNPK interact with each other (Kim et al., 2000), and they interact as part of a complex in murine ESCs (Lin et al., 2014). We then investigated whether PTBP1 and HNRNPK are functionally related to *Lncenc*1. As expected, knockdown of *Ptbp1* or *Hnrnpk* resulted in a significant downregulation of pluripotency and glycolysis genes (Figures 6C and 6D) and a significant reduction of glucose consumption and lactate production (Figure 6E), which is consistent with phenotypes observed in *the Lncenc1* knockdown or KO cells. These data indicated that *Lncenc1*,

---

(E and F) Expression dynamics of two pluripotency genes (*Oct4* and *Nanog*) and *Lncenc1* during the nESC-to-EpiLC transition (E), and during spontaneous differentiation (F). Expression levels were normalized against *Actb*. Results are shown as means ± SD of three independent experiments. Data are compared with 0 hr. Statistical significance of t test: *p < 0.05, **p < 0.01, ***p < 0.001.
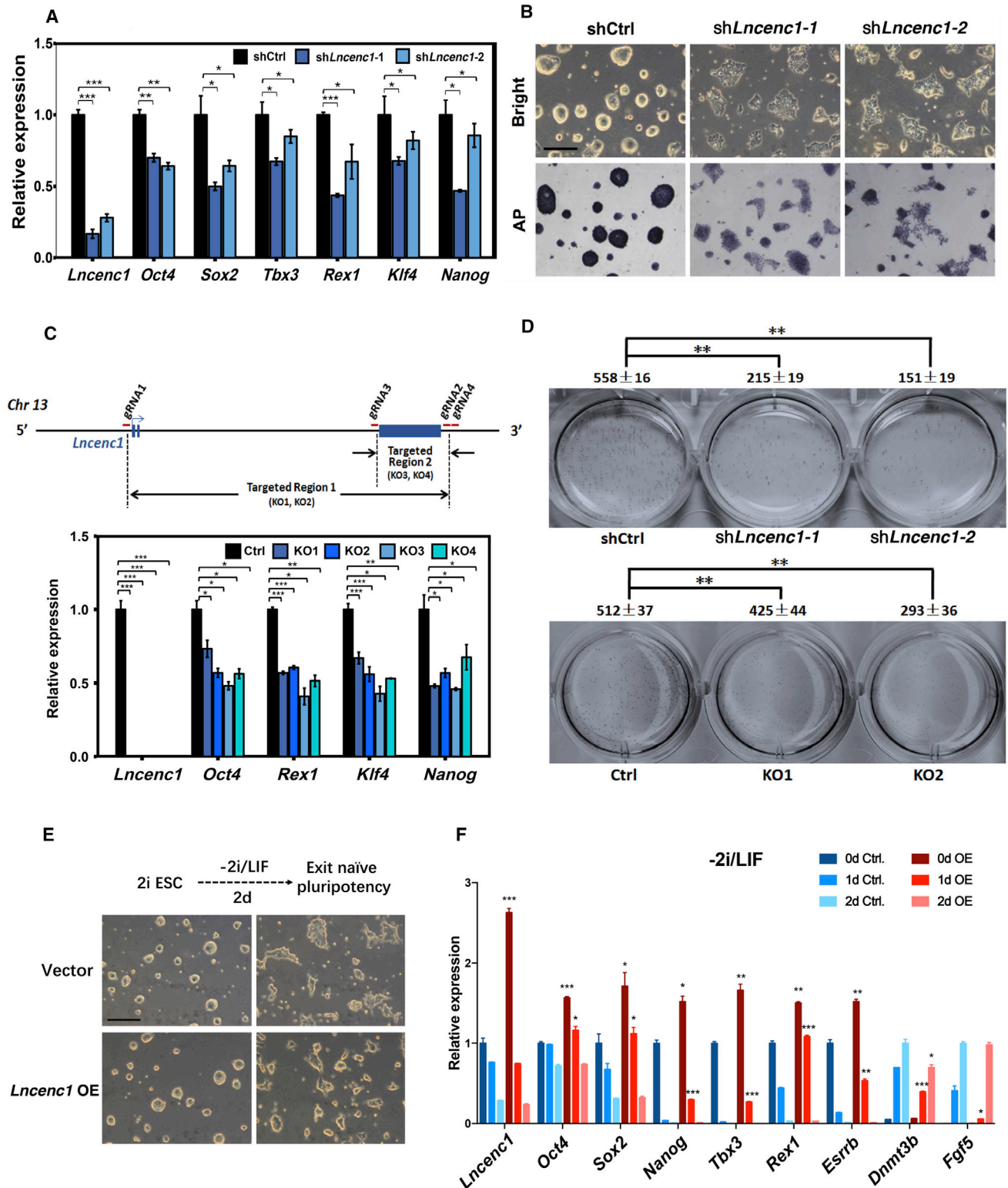See also Figures S2B and S2C.

Figure 3. *Lncenc1* Is Required to Maintain the Self-Renewal of Mouse nESCs

(A) Expression levels of six pluripotency genes as measured by qRT-PCR in nESCs upon shRNA-mediated knockdown of *Lncenc1*. Expression levels were normalized against *Actb*. Results are shown as means ± SD of three independent experiments. Statistical significance of t test: *p < 0.05, **p < 0.01, ***p < 0.001.

(legend continued on next page)

PTBP1, and HNRNPK are interacting physically and functionally.

To test whether the *Lncenc1*-PTBP1-HNRNPK complex regulates the expression of pluripotency and/or glycolysis genes, we performed chromatin immunoprecipitation (ChIP) experiments in *Lncenc1* knockdown and control nESCs. Indeed, HNRNPK binds to the promoters of pluripotency and glycolysis genes. However, only the occupancy of HNRNPK on glycolytic genes, but not pluripotency genes, were significantly decreased in knockdown cells compared with the control cells (Figure 6F). Furthermore, the occupancy of RNA polymerase II on glycolysis gene promoters decreased significantly upon *Lncenc1* or PTBP1 knockdown (Figures 6G and S5). In addition, we performed chromatin isolation by RNA purification (ChIRP) assay in *Lncenc1* knockout and control nESCs. Consistent with our ChIP data, *Lncenc1* occupied the promoters at four of the five glycolytic genes (Figure 6H). These data suggested that *Lncenc1* guides HNRNPK and PTBP1 binding to glycolysis genes; therefore promoting their levels of transcription.

Interplays among *Lncenc1*, Core Pluripotency Networks, and Glycolytic Genes

Given that *Lncenc1* can affect self-renewal and glycolysis, we were curious about the regulatory relationships among them. First, upon the knockdown of the individual pluripotency gene (*Oct4*, *Sox2*, *Nanog*, or *Klf4*) (Figure S6A), *Lncenc1* and all examined glycolysis genes were downregulated consistently (Figure 7A). Second, a recent study showed that core pluripotency factors directly regulate expression of glycolysis genes (Kim et al., 2015), and that the *Lncenc1* locus is enriched for the binding of OCT4 (Figure 1C), indicating that *Lncenc1* and glycolysis genes are regulated directly by core pluripotency factors.

In contrast, knockdown of individual glycolysis genes failed to downregulate *Lncenc1* and pluripotency genes, except for *Klf4* (Figures 7B and S6B). However, when all these five glycolysis genes were knocked down together (with two sets of shRNA pools), *Lncenc1* and pluripotency genes were all markedly declined (Figures 7C, S6C, and S6D). Furthermore, the adding of 2-deoxy-D-glucose (2-DG) (a glycolysis inhibitor) to the 2i/LIF medium leads to "flatter" clone morphology and significant decreases of pluripotency gene expression (Figure S6E). These data suggested that the glycolysis pathway, rather than individual genes, regulates the core pluripotency genes.

In summary, our data suggested that *Lncenc1*, PTBP1, and HNRNPK form functional complexes, which promote expression of glycolysis genes, thereby maintaining the glycolytic activity, which is required for the self-renewal of naive ESCs (Figure 7D).

DISCUSSION

Functional studies indicated that some lncRNAs regulate self-renewal or pluripotency through integrating or disturbing core pluripotency networks. For example, *Gomafu* regulates *Oct4* and *Nanog* expression through the formation of a positive feedback loop with *Oct4* (Sheik Mohamed et al., 2010), and *TUNA* maintains self-renewal of mESCs through promoting transcriptional activities of pluripotent genes including *Nanog*, *Sox2*, and *Fgf4* (Kaneko et al., 2014). However, an *Oct4* pseudogene lncRNA guides SUV39H1, a repressive chromatin modifier, to the promoter and epigenetically silences the *Oct4* gene in differentiated cells (Scarola et al., 2015). Similarly, in somatic cells, lincRNA-p21 interacts with SETDB1, which silences pluripotency genes by depositing histone H3K9me3 on their promoters (Bao et al., 2015). Furthermore, linc-ROR promotes reprogramming by repressing pathways including P53 responses (Loewer et al., 2010), and this lncRNA maintains self-renewal of human ESCs through sponging miR-145, which targets mRNAs of core pluripotency genes (Wang et al., 2013). Recently, Austin Smith and colleagues reported that the lncRNA *Ephemeron* modulates the exit from naive pluripotency by connecting microRNA and *de novo* DNA

(B) Bright-field micrographs (upper panels) and alkaline phosphatase staining in control nESCs and *Lncenc1* knockdown ESCs. Scale bars, 200 μm. See also Figure S3C.

(C) Expression of pluripotency genes in wild-type (Ctrl.) and *Lncenc1* KO nESCs. Upper panel: the schematic representation of CRISPR/Cas9-mediated knockouts of the *Lncenc1* locus. Four KO clones were obtained by depletion of the whole gene (KO1 and KO2) or depletion of the largest exon (KO3 and KO4). Expression levels were normalized against *Actb*. Results are shown as means ± SD of three independent experiments. Statistical significance of t test: *p < 0.05, **p < 0.01, ***p < 0.001.

(D) Results of colony formation experiments in control and *Lncenc1* knockdown or KO nESCs. Clone numbers are shown as means ± SD of three replicates. Statistical significance of t test: **p < 0.01.

(E) Bright-field micrographs of control nESCs and *Lncenc1*-overexpressed ESCs in 2I/LIF (left) and then withdrawal of 2i/LIF for 2 days (right). Scale bars, 200 μm.

(F) Expression levels of pluripotency genes of control nESCs and *Lncenc1*-overexpressed ESCs in 2i/LIF (0d) and spontaneous differentiation (1d, 2d). Expression levels were normalized against *Actb*. Results are shown as means ± SD of three independent experiments. Statistical significance of t test: *p < 0.05, **p < 0.01, ***p < 0.001.
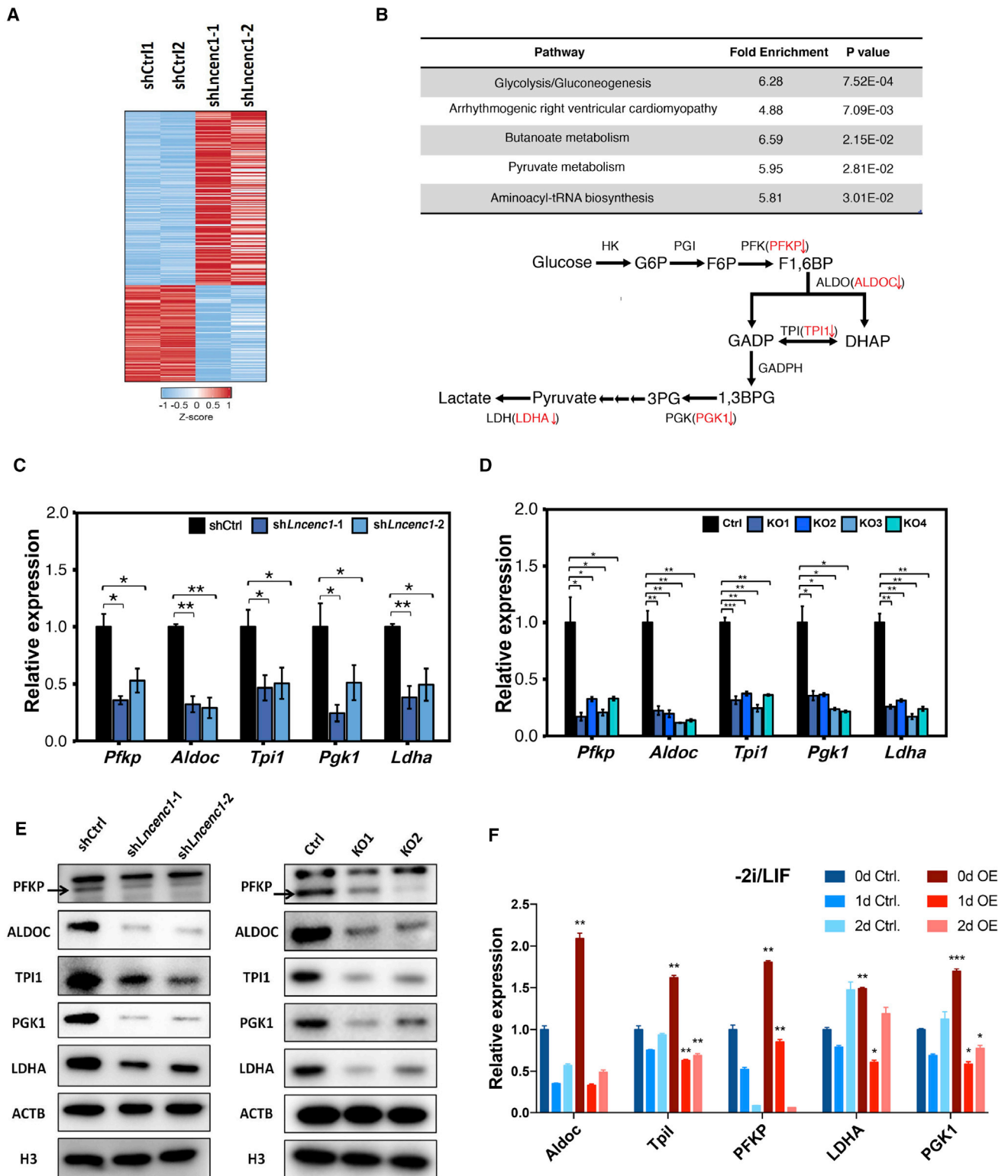
Figure 4. *Lncenc1* Regulates the Glycolysis Pathway in nESCs

(A) The heatmap of differentially expressed genes upon *Lncenc1* knockdown as identified by RNA-seq experiments.

(B) Significantly enriched pathways (p < 0.05) of differentially expressed genes upon *Lncenc1* knockdown as revealed by KEGG pathway analysis. Lower panel: the schematic showing of the glycolysis pathway and significantly downregulated genes (in red) upon *Lncenc1* depletion.
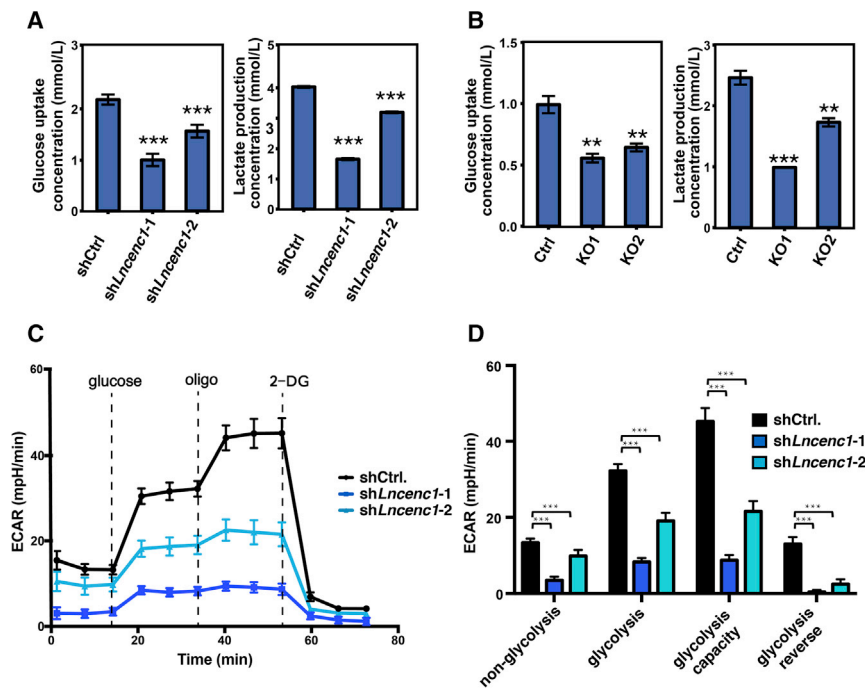
(legend continued on next page)

Figure 5. Glycolic Activity Decreases upon *Lncenc1* Depletion

(A and B) Measurements of glucose uptake and lactate production in *Lncenc1* knockdown (A) or KO (B) nESCs. Shown are results of three replicates (means ± SD). Statistical significance of t test: **p < 0.01, ***p < 0.001.

(C and D) Results of glycolysis stress tests as measured by the glucose-dependent extracellular acidification rate (ECAR). Shown are measurements of at least five replicates (means ± SD). Statistical significance of t test: ***p < 0.001.

methylation (Bates and Silva, 2017). In this study, we demonstrate that *Lncenc1* maintains self-renewal by regulating the glycolysis pathway. To our knowledge, *Lncenc1* is the first lncRNA linking self-renewal and energy metabolism in PSCs.

We showed that *Lncenc1* interacts with two RNA binding proteins (RBPs), PTBP1 and HNRNPK. Interestingly, the lncRNA *TUNA* also interacts with PTBP1 and HNRNPK, activating pluripotency genes directly (Kaneko et al., 2014). However, *linc-p21* interacts with HNRNPK and SETBD1, silencing rather than activating its target genes in somatic cells (Bao et al., 2015). PTBP1 is required for embryonic development (Suckale et al., 2011), and HNRNPK could interact with multiple proteins through its K interactive region to play various roles in diverse cellular processes (Geuens et al., 2016). Based on these data, we propose that a class of RBPs such as HNRNPK could form complexes with different lncRNAs and/or proteins that regulate specific classes of genes in different cell types. Further investiga-

tions are needed to reveal the functions of lncRNA-RBP complexes in various biological systems.

Recently, energy metabolism has been closely linked to stem cell fates. For example, during the ESC-to-EpiSC transition, energy metabolism switched from bivalent (utilization of both glycolysis and oxidative phosphorylation) to exclusively glycolytic, and hypoxia inducible factor 1a was sufficient to drive ESC to an EpiSC-like stage (Zhou et al., 2012). A recent metabolome analysis further indicated that, although early metabolites are increased, downstream glycolysis metabolites are decreased in primed hESCs (Sperber et al., 2015). Interestingly, when mESCs adapted from serum to 2i conditions, the glycolysis pathway was significantly upregulated as detected by RNA-seq (Marks et al., 2012). Similarly, protein levels of glycolysis enzymes are significantly increased in naive ESCs compared with ESCs cultured in serum (Taleahmad et al., 2015). Our data further demonstrate that the downregulation of glycolysis by *lncenc1* depletion impairs

(C and D) Expression of glycolysis genes in the *Lncenc1* knockdown or KO nESCs. (C) knockdown by shRNAs; (D) KO by CRISPR/Cas9. Data were normalized against *Actb* and are shown as means ± SD of three independent experiments. Statistical significance of t test: *p < 0.05, **p < 0.01, ***p < 0.001. See also Figure S3B.

(E) Protein levels of glycolytic enzymes in *Lncenc1* knockdown (left) or KO (right) nESCs as detected by western blot analysis. ACTB and H3 were used as the loading controls.

(F) Expression levels of glycolysis genes in control and *Lncenc1*-overexpressed ESCs in 2i/LIF (0d) and spontaneous differentiation (1d, 2d). Data were normalized against *Actb* and are shown as means ± SD of three independent experiments. Statistical significance of t test: *p < 0.05, **p < 0.01, ***p < 0.001.
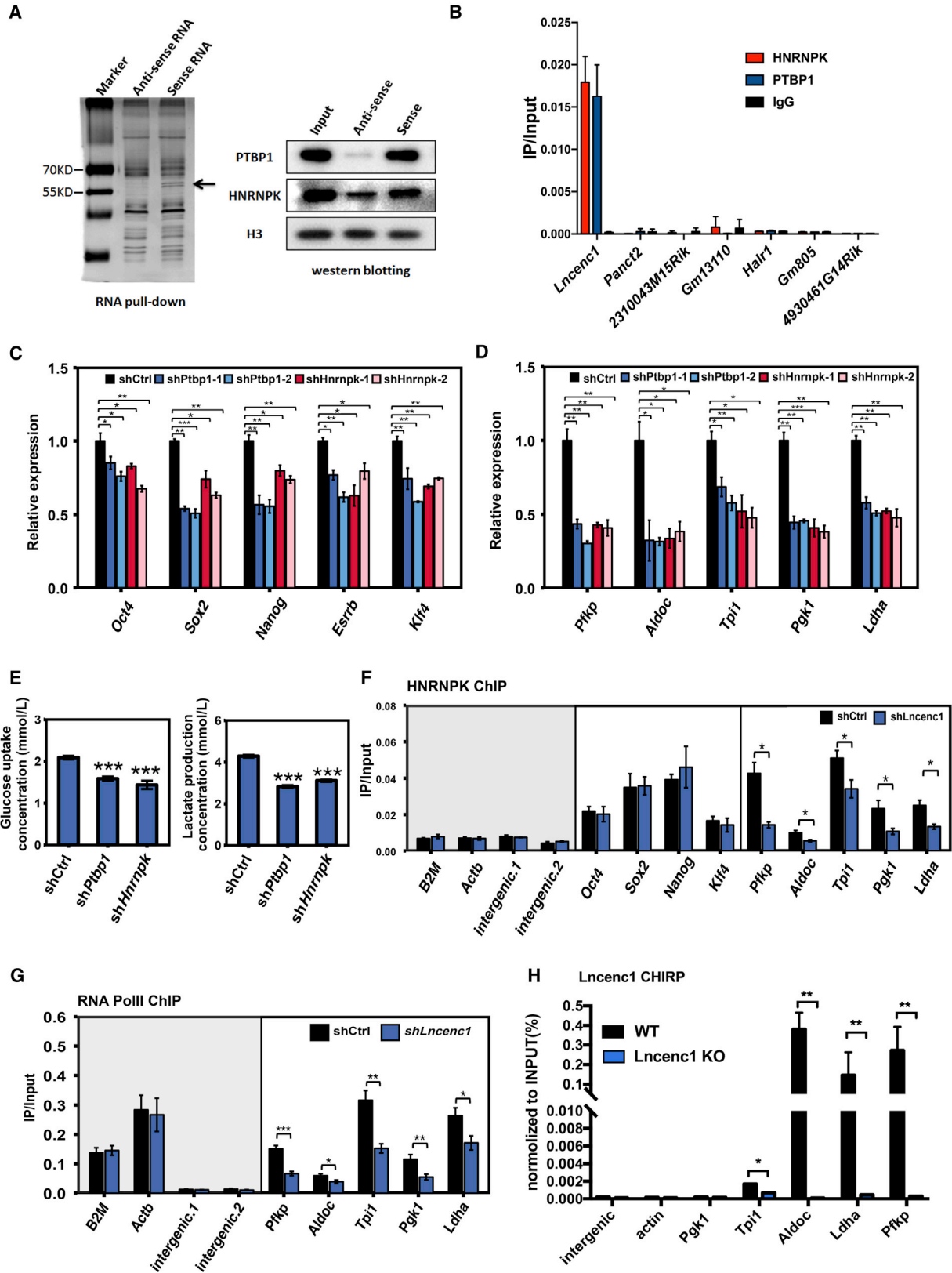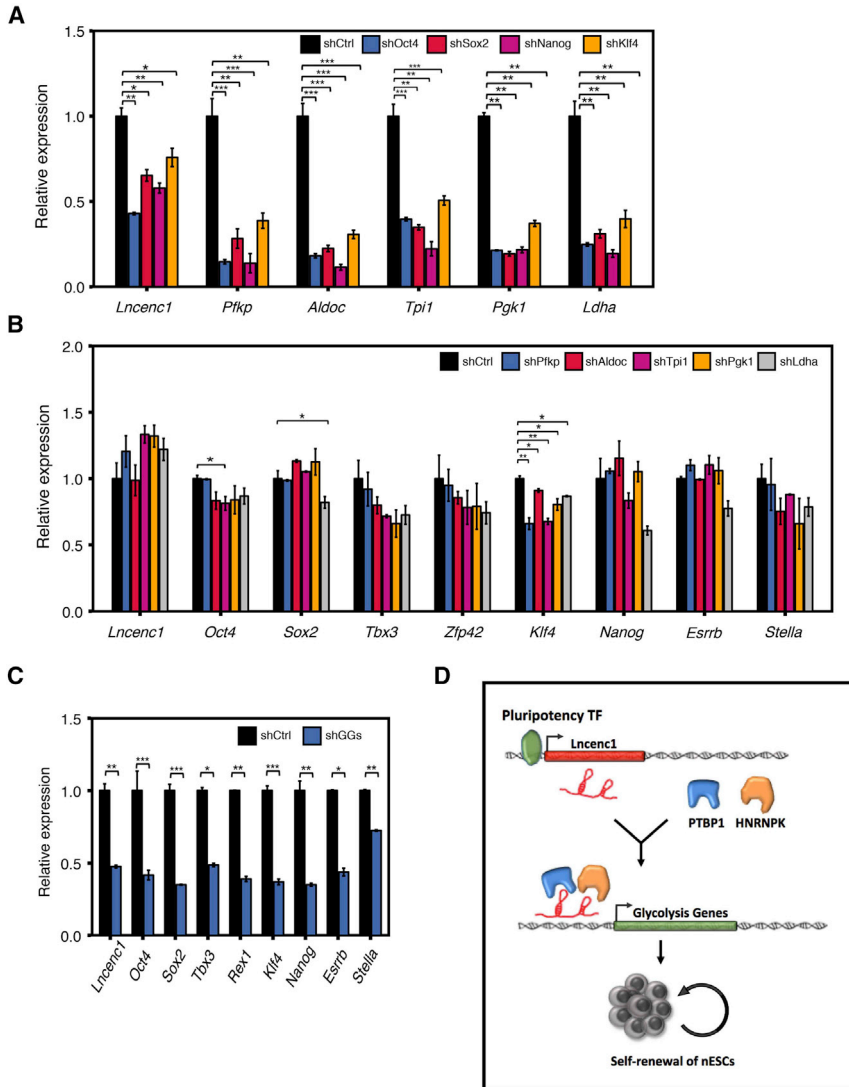
(legend on next page)

Figure 7. Regulatory Relationships among *Lncenc1*, Pluripotency Genes, and Glycolysis Genes

(A–C) Expression of *Lncenc1* and glycolysis genes when individual pluripotency genes were knocked down (A); expression of *Lncenc1* and pluripotency genes when individual glycolysis genes were knocked down (B); and expression of *Lncenc1* and pluripotency genes upon knockdown of all five glycolysis genes (GGs) (C). For qRT-PCR experiments, expression levels were normalized against *Actb*, and data are shown as means ± SD of three independent experiments. Statistical significance of t test: *p < 0.05, **p < 0.01, ***p < 0.001.

(D) Working model of *Lncenc1* in nESCs.

self-renewal, which suggests that a high level of glycolysis is vital for naive ESCs. However, it remains unclear how glycolysis regulates naive pluripotency. It is possible that

a faster generation of ATPs by glycolysis benefits highly proliferative cells including stem cells and cancer cells, or that glycolysis-generated metabolites are essential for

Figure 6. *Lncenc1* Associates with HNRNPK and PTBP1 Functionally

(A) Results of RNA pull-down experiments. Biotinylated *Lncenc1* sense or antisense RNAs were used for the experiments. Two specific bands (arrowheads) were excised and subjected to mass spectrometry analysis, and were further validated by western blotting.

(B) RNA immunoprecipitation (RIP) with anti-HNRNPK and anti-PTBP1 antibodies in E14 nESCs. Enrichments of lncRNAs, i.e., expression of RIP relative to input samples, were determined by qRT-PCR.

(C and D) Expression of pluripotency genes (C) or glycolysis genes (D) upon knockdown of *Ptbp1* and *Hnrnpk*. Data were normalized against *Actb*, and shown as the means ± SD of three independent experiments. Statistical significance of t test: *p < 0.05, **p < 0.01, ***p < 0.001.

(E) Glycolysis signatures of Hnrnpk and Ptbp1 knockdown cells. Data were presented as means ± SD.

(F–H) Chromatin immunoprecipitation (ChIP) experiments with HNRNPK (F) or RNA polymerase II (G) antibodies; CHIRP experiment with specific anti-*Lncenc1* probes (H). Relative enrichment of ChIP or CHIRP and input DNA were determined by qPCR. Primers were designed at promoters of glycolysis genes, pluripotency genes, and control genes (*B2m* and *Actb*), and two intergenic regions were used as negative controls. Data are shown as means ± SD of three independent experiments. Statistical significance of t test: *p < 0.05, **p < 0.01, ***p < 0.001.

establishing the epigenetic modifications required for the maintenance of PSCs (Lin et al., 2016; Moussaieff et al., 2015; Sperber et al., 2015). Further investigations are required to decipher the detailed mechanisms underlying glycolysis and naive pluripotency states. Moreover, it would be possible to optimize culture systems for PSCs by manipulating metabolic status by adding or removing specific glycolysis metabolites.

Nevertheless, it remains elusive how *Lncenc1* functions *in vivo*, and developing *Lncenc1*-deficient mouse models will be critical in addressing this question. *Lncenc1* RNAs locate both in nucleus and cytoplasm. In this study, we investigated the functions of the nuclear *Lncenc1*, yet the activity of cytoplasmic *Lncenc1* remains to be explored in the future. Finally, as exemplified by *Lncenc1* and other lncRNAs regulating glycolysis in cancer (Bao et al., 2015; Dowen et al., 2014; Geuens et al., 2016; Rupaimoole et al., 2015), it would be interesting to explore further functional roles of different lncRNAs in regulating energy metabolism in stem cells, development, and diseases.

EXPERIMENTAL PROCEDURES

Cell Culture
To maintain ESCs in ground state or naive state, cells from two mouse ESC lines (E14TG2a and R1) were cultured in 2i /LIF conditions as described (Li et al., 2008). The nESC-to-EpiLC transition was conducted as described (Hayashi et al., 2011) with minor modifications. For spontaneous differentiation, nESC cells were plated at a density of 1×10^4 per cm^2 in gelatin-coated plates in N2B27 medium without 2i/LIF for 4 days. For the 2-DG treatment, nESCs were cultured in 2i/LIF medium for 1 day and then treated with 2-DG (100 mM) for 2 days.

RNA-Seq and Data Analysis
Total RNA was prepared with TRIzol reagents (Life Technologies). For RNA-seq experiments, rRNA-depleted and strand-specific libraries were constructed with the Ribo-zero gold (Epicentre) and TruSeq Stranded Total RNA Sample Prep Kit (Illumina), and the libraries were sequenced using the HighSeq 2000 system (Illumina). The analyses of RNA-seq data, including raw data processing, mapping, and gene expression, were conducted as described previously (Fan et al., 2018). For differential gene expression analysis, we analyzed raw read counts for GENCODE M7 gene models using the HTSeq software (Anders et al., 2015), and then calculated statistics of DE via DESeq2 (Love et al., 2014) with default parameters. To define differentially expressed genes, we used a false discovery rate of 0.05 (ESC-EpiLC comparison) or 0.1 (*Lncenc1* knockdown studies) as thresholds. We performed KEGG pathway analysis using DAVID bioinformatics tools as described (Huang da et al., 2009).

Northern Blot Analysis
For northern blotting, 10 μg of total RNAs was mixed with 2× loading buffer (Fermentas), incubated at 55°C for 5 min, and resolved by denaturing agarose gel electrophoresis; the RNAs were then transferred to a nylon membrane and crosslinked by UV irradiation. Digoxigenin-labeled RNA probe preparation, hybridization, and detection were conducted via a DIG Northern Starter Kit (Roche) according to the manufacturer's protocol.

Cellular Fractionation
Cellular fractionation experiments were performed with 1×10^7 nESCs as described previously (Bhatt et al., 2012).

Gene Knockdown
The shRNA-based knockdown experiments were conducted as described previously (Bao et al., 2015). The validated shRNA sequences were provided in Table S3. For ASO-mediated knockdown, we used phosphorothioate-modified oligodeoxynucleotides (Ideue et al., 2009). Two independent ASOs targeting *Lncenc1* (mUm CmCmUmUAAGGTGCTTCmAmGmTmTmC, and mGmUmCm AmUGCTGATGCTGmGmUmGmCmA), and one control ASO (mCmCmUmUmCCCTGAAGGTTmCmCmUmCmC) were synthesized (BioSune). Then 2×10^5 nESCs were transfected with 100 μM of each ASO with 6 μL RNAiMAX (Life Technologies) and harvested 48 hr after the transfection.

Gene Knockout
To deplete the *Lncenc1* locus in E14 ESCs, we applied CRISPR/Cas9-based assays as described (Cong et al., 2013). Two pairs of guide RNAs (pair1: GAGCCAATCTCTAGGCAAGT and GTATGACAA ATGCTTATTGA; pair2: GTGCTTTTGTGTTATCCCGG and GGTCC ATTATGTAACCACCT) were used to target the *Lncenc1* genomic locus, deleting regions about 15 kb (pair1) and 3 kb (pair2), respectively. *Lncenc1* knockouts were verified by genomic DNA PCR and sequencing.

Overexpression
The *Lncenc1* cDNA was cloned into the pcDNA3.1 vector, and the overexpression experiments were performed with electroporation by the Neon system (Invitrogen), according to the manufacturer's instructions.

qRT-PCR
The qRT-PCR experiments were conducted as described (Bao et al., 2015). Primer sequences for qRT-PCR are listed in Table S4.

Western Blotting
Total cell lysates were prepared in 1× SDS buffer. An equal amount of proteins were separated by SDS-PAGE gel electrophoresis and transferred onto polyvinylidene difluoride membranes. The following antibodies were used for western blotting: anti-HNRNPK (Abcam, ab39975), anti-PTBP1 (Invitrogen, 324800), anti-PFKP (Proteintech, 13,389), anti-ALDOC (Proteintech, 14,884), anti-TPI1 (Proteintech, 10,713), anti-LDHA (Proteintech, 14,824), anti-PGK1 (Proteintech, 17,811), anti-SOX2 (Proteintech, 11,064), anti-H3 (Abcam, ab1791), anti-ACTB (Proteintech, 60,008-1-Ig), OCT4 (Santa Cruz, sc-8628). The blots were developed with ECL Plus Western Blotting Substrate (Thermo Scientific), and imaged by the FluorChem M System (ProteinSimple).

RNA Fluorescence *In Situ* Hybridization

RNA fluorescence *in situ* hybridization for the detection of *Lncenc1* and *Ppib* (positive control) was performed using an RNAscope (Advanced Cell Diagnostics, Hayward, CA, 323100), according to the protocol provided by the manufacturer.

Alkaline Phosphatase Detection

ESCs were fixed with 4% paraformaldehyde and stained with the Alkaline Phosphatase Staining Kit (Millipore) according to the manufacturer's protocol.

Colony Formation

ESCs were plated at a density of 100 per cm^2 in laminin-coated 6-well plates in 2i/LIF. The medium was changed every 3 days. After 6 days, colonies were fixed and stained for alkaline phosphatase. Colonies were counted using the ImageJ software.

The Measurement of Glucose Uptake and Lactate Production

The same amount (1 $\times$ 10^6) of control and knockdown or knockout ESCs were seeded on a well of 12-well plates in 0.5 mL of N2B27 medium containing 2i/LIF. After 6 hr, the culture medium was collected for glucose and lactate measurement, using the Cobas C311 Chemistry Analyzer (Roche), according to the manufacturer's instructions. The intracellular glucose consumption and lactate production were calculated by the concentration differences between cultured medium and the blank medium.

Seahorse XF Bioenergetic Analysis

SeaHorse plates were pre-treated by coating with 0.1% gelatin. ECAR in mESCs were measured using the Seahorse XF96 bio-analyzer according to the manufacturer's protocols. Cells were seeded in an XF96 microplate at a density of 20,000 cells per well. Culture medium was changed to unbuffered XF assay medium at pH 7.4 (Seahorse Biosciences), supplemented with 5.5 mM glucose (Sigma) and 1 mM pyruvate for assay of glycolysis rates. Before assay, the microplate was transferred into a non-CO2 incubator at 37°C for 60 min. For the glycolysis stress test, after collecting baseline acidification rate data, cells were sequentially treated with 10 mM glucose, 1 mM oligomycin, and 50 mM 2-DG, and the subsequent changes were quantified. All metabolic profiles were normalized to cell numbers.

RNA Pull-Down Assay

RNA pull-down experiments were performed as described previously (Tsai et al., 2010). Specific gel bands were excised and subject to mass spectrometry analysis.

RNA Immunoprecipitation

Mouse nESCs (1 $\times$ 10^7) were subjected to nuclei isolation as described (Doi et al., 2009). Nuclei were then resuspended in 1 mL of cold RNA immunoprecipitation (RIP) buffer (150 mM KCl, 25 mM Tris [pH 7.4], 5 mM EDTA, 0.5 mM DTT, 0.5% NP40, 100 U/mL RNAase inhibitor, 1× Complete) and sheared by sonication. For immunoprecipitation (IP), 2 μg of specific antibody (HNRNPK [Abcam, ab39975]; PTBP1 [Invitrogen, 324800]) or the

control IgG (Cell Signaling Technologies, 2,729) was incubated with 6–10 mg supernatant at 4°C for 2 hr, then 20 μL of protein G magnetic beads (Invitrogen) were added to each IP sample and incubated at 4°C for 1 hr. The beads were collected and washed three times with RIP buffer. RNAs were extracted with TRIzol, and enrichment for each gene was determined by qRT-PCR.

ChIP

ChIP experiments were performed with 1 $\times$ 10^7 mESCs as described previously (Irizarry et al., 2008). The following antibodies were used for ChIP: anti-HNRNPK (Abcam, ab39975) and anti-RNA PolII (Abcam, ab817). Primers for ChIP-PCR were provided in Table S5.

ChIRP

ChIRP experiments were performed as described previously (Chu et al., 2011). Probe sequences are provided in Table S6.

ACCESSION NUMBERS

The RNA-seq datasets from this study have been submitted to the NCBI GEO (http://www.ncbi.nlm.nih.gov/geo/) under accession number GEO: GSE116602.

SUPPLEMENTAL INFORMATION

Supplemental Information includes six figures and six tables and can be found with this article online at https://doi.org/10.1016/j.stemcr.2018.08.001.

AUTHOR CONTRIBUTIONS

Z.S., M.Z., L.C., and B.W. conceived and designed the study. Z.S., M.Z., L.C., Q.W., P.T., and Z.Y. performed the experiments. P.L. performed bioinformatics analysis. All authors reviewed and approved the manuscript.

ACKNOWLEDGMENTS

REFERENCES

Anders, S., Pyl, P.T., and Huber, W. (2015). HTSeq – a Python framework to work with high-throughput sequencing data. Bioinformatics *31*, 166–169.

Bao, X., Wu, H., Zhu, X., Guo, X., Hutchins, A.P., Luo, Z., Song, H., Chen, Y., Lai, K., Yin, M., et al. (2015). The p53-induced

lincRNA-p21 derails somatic cell reprogramming by sustaining H3K9me3 and CpG methylation at pluripotency gene promoters. Cell Res. *25*, 80–92.

Bates, L.E., and Silva, J.C. (2017). Reprogramming human cells to naive pluripotency: how close are we? Curr. Opin. Genet. Dev. *46*, 58–65.

Bergmann, J.H., Li, J., Eckersley-Maslin, M.A., Rigo, F., Freier, S.M., and Spector, D.L. (2015). Regulation of the ESC transcriptome by nuclear long noncoding RNAs. Genome Res. *25*, 1336–1346.

Bhatt, D.M., Pandya-Jones, A., Tong, A.J., Barozzi, I., Lissner, M.M., Natoli, G., Black, D.L., and Smale, S.T. (2012). Transcript dynamics of proinflammatory genes revealed by sequence analysis of subcellular RNA fractions. Cell *150*, 279–290.

Brons, I.G., Smithers, L.E., Trotter, M.W., Rugg-Gunn, P., Sun, B., Chuva de Sousa Lopes, S.M., Howlett, S.K., Clarkson, A., Ahrlund-Richter, L., Pedersen, R.A., et al. (2007). Derivation of pluripotent epiblast stem cells from mammalian embryos. Nature *448*, 191–195.

Chu, C., Qu, K., Zhong, F.L., Artandi, S.E., and Chang, H.Y. (2011). Genomic maps of long noncoding RNA occupancy reveal principles of RNA-chromatin interactions. Mol. Cell *44*, 667–678.

Cong, L., Ran, F.A., Cox, D., Lin, S., Barretto, R., Habib, N., Hsu, P.D., Wu, X., Jiang, W., Marraffini, L.A., et al. (2013). Multiplex genome engineering using CRISPR/Cas systems. Science *339*, 819–823.

da Rocha, S.T., Boeva, V., Escamilla-Del-Arenal, M., Ancelin, K., Granier, C., Matias, N.R., Sanulli, S., Chow, J., Schulz, E., Picard, C., et al. (2014). Jarid2 is implicated in the initial xist-induced targeting of PRC2 to the inactive x chromosome. Mol. Cell *53*, 301–316.

De Los Angeles, A., Ferrari, F., Xi, R., Fujiwara, Y., Benvenisty, N., Deng, H., Hochedlinger, K., Jaenisch, R., Lee, S., Leitch, H.G., et al. (2015). Hallmarks of pluripotency. Nature *525*, 469–478.

Doi, A., Park, I.H., Wen, B., Murakami, P., Aryee, M.J., Irizarry, R., Herb, B., Ladd-Acosta, C., Rho, J., Loewer, S., et al. (2009). Differential methylation of tissue- and cancer-specific CpG island shores distinguishes human induced pluripotent stem cells, embryonic stem cells and fibroblasts. Nat. Genet. *41*, 1350–1353.

Dowen, J.M., Fan, Z.P., Hnisz, D., Ren, G., Abraham, B.J., Zhang, L.N., Weintraub, A.S., Schuijers, J., Lee, T.I., Zhao, K., et al. (2014). Control of cell identity genes occurs in insulated neighborhoods in mammalian chromosomes. Cell *159*, 374–387.

Evans, M.J., and Kaufman, M.H. (1981). Establishment in culture of pluripotential cells from mouse embryos. Nature *292*, 154–156.

Fan, H., Lv, P., Huo, X., Wu, J., Wang, Q., Cheng, L., Liu, Y., Tang, Q.Q., Zhang, L., Zhang, F., et al. (2018). The nuclear matrix protein HNRNPU maintains 3D genome architecture globally in mouse hepatocytes. Genome Res. *28*, 192–202.

Flynn, R.A., and Chang, H.Y. (2014). Long noncoding RNAs in cell-fate programming and reprogramming. Cell Stem Cell *14*, 752–761.

Geuens, T., Bouhy, D., and Timmerman, V. (2016). The hnRNP family: insights into their role in health and disease. Hum. Genet. *135*, 851–867.

Guo, G., von Meyenn, F., Santos, F., Chen, Y., Reik, W., Bertone, P., Smith, A., and Nichols, J. (2016). Naive pluripotent stem cells derived directly from isolated cells of the human inner cell mass. Stem Cell Reports *6*, 437–446.

Guttman, M., Amit, I., Garber, M., French, C., Lin, M.F., Feldser, D., Huarte, M., Zuk, O., Carey, B.W., Cassady, J.P., et al. (2009). Chromatin signature reveals over a thousand highly conserved large non-coding RNAs in mammals. Nature *458*, 223–227.

Guttman, M., Donaghey, J., Carey, B.W., Garber, M., Grenier, J.K., Munson, G., Young, G., Lucas, A.B., Ach, R., Bruhn, L., et al. (2011). lincRNAs act in the circuitry controlling pluripotency and differentiation. Nature *477*, 295–300.

Hackett, J.A., and Surani, M.A. (2014). Regulatory principles of pluripotency: from the ground state up. Cell Stem Cell *15*, 416–430.

Hayashi, K., Ohta, H., Kurimoto, K., Aramaki, S., and Saitou, M. (2011). Reconstitution of the mouse germ cell specification pathway in culture by pluripotent stem cells. Cell *146*, 519–532.

Huang da, W., Sherman, B.T., and Lempicki, R.A. (2009). Systematic and integrative analysis of large gene lists using DAVID bioinformatics resources. Nat. Protoc. *4*, 44–57.

Ideue, T., Hino, K., Kitao, S., Yokoi, T., and Hirose, T. (2009). Efficient oligonucleotide-mediated degradation of nuclear noncoding RNAs in mammalian cultured cells. RNA *15*, 1578–1587.

Irizarry, R.A., Ladd-Acosta, C., Carvalho, B., Wu, H., Brandenburg, S.A., Jeddeloh, J.A., Wen, B., and Feinberg, A.P. (2008). Comprehensive high-throughput arrays for relative methylation (CHARM). Genome Res. *18*, 780–790.

Jain, A.K., Xi, Y., McCarthy, R., Allton, K., Akdemir, K.C., Patel, L.R., Aronow, B., Lin, C., Li, W., Yang, L., et al. (2016). LncPRESS1 is a p53-regulated LncRNA that safeguards pluripotency by disrupting SIRT6-mediated de-acetylation of histone H3K56. Mol. Cell *64*, 967–981.

Kalkan, T., and Smith, A. (2014). Mapping the route from naive pluripotency to lineage specification. Philos. Trans. R. Soc. B Biol. Sci. *369*. https://doi.org/10.1098/rstb.2013.0540.

Kaneko, S., Bonasio, R., Saldana-Meyer, R., Yoshida, T., Son, J., Nishino, K., Umezawa, A., and Reinberg, D. (2014). Interactions between JARID2 and noncoding RNAs regulate PRC2 recruitment to chromatin. Mol. Cell *53*, 290–300.

Kelley, D., and Rinn, J. (2012). Transposable elements reveal a stem cell-specific class of long noncoding RNAs. Genome Biol. *13*, R107.

Kim, H., Jang, H., Kim, T.W., Kang, B.H., Lee, S.E., Jeon, Y.K., Chung, D.H., Choi, J., Shin, J., Cho, E.J., et al. (2015). Core pluripotency factors directly regulate metabolism in embryonic stem cell to maintain pluripotency. Stem Cells *33*, 2699–2711.

Kim, J.H., Hahm, B., Kim, Y.K., Choi, M., and Jang, S.K. (2000). Protein-protein interaction among hnRNPs shuttling between nucleus and cytoplasm. J. Mol. Biol. *298*, 395–405.

Kurimoto, K., Yabuta, Y., Hayashi, K., Ohta, H., Kiyonari, H., Mitani, T., Moritoki, Y., Kohri, K., Kimura, H., Yamamoto, T., et al. (2015). Quantitative dynamics of chromatin remodeling during germ cell specification from mouse embryonic stem cells. Cell Stem Cell *16*, 517–532.

Lennox, K.A., and Behlke, M.A. (2016). Cellular localization of long non-coding RNAs affects silencing by RNAi more than by antisense oligonucleotides. Nucleic Acids Res. *44*, 863–877.

Li, P., Tong, C., Mehrian-Shai, R., Jia, L., Wu, N., Yan, Y., Maxson, R.E., Schulze, E.N., Song, H., Hsieh, C.L., et al. (2008). Germline competent embryonic stem cells derived from rat blastocysts. Cell *135*, 1299–1310.

Lin, A., Li, C., Xing, Z., Hu, Q., Liang, K., Han, L., Wang, C., Hawke, D.H., Wang, S., Zhang, Y., et al. (2016). The LINK-A lncRNA activates normoxic HIF1alpha signalling in triple-negative breast cancer. Nat. Cell. Biol. *18*, 213–224.

Lin, N., Chang, K.Y., Li, Z., Gates, K., Rana, Z.A., Dang, J., Zhang, D., Han, T., Yang, C.S., Cunningham, T.J., et al. (2014). An evolutionarily conserved long noncoding RNA TUNA controls pluripotency and neural lineage commitment. Mol. Cell *53*, 1005–1019.

Liu, J., Li, Y., Lin, B., Sheng, Y., and Yang, L. (2017). HBL1 is a human long noncoding RNA that modulates cardiomyocyte development from pluripotent stem cells by counteracting MIR1. Dev. Cell *42*, 333–348 e35.

Loewer, S., Cabili, M.N., Guttman, M., Loh, Y.H., Thomas, K., Park, I.H., Garber, M., Curran, M., Onder, T., Agarwal, S., et al. (2010). Large intergenic non-coding RNA-RoR modulates reprogramming of human induced pluripotent stem cells. Nat. Genet. *42*, 1113–1117.

Love, M.I., Huber, W., and Anders, S. (2014). Moderated estimation of fold change and dispersion for RNA-seq data with DESeq2. Genome Biol. *15*, 550.

Luo, S., Lu, J.Y., Liu, L., Yin, Y., Chen, C., Han, X., Wu, B., Xu, R., Liu, W., Yan, P., et al. (2016). Divergent lncRNAs regulate gene expression and lineage differentiation in pluripotent cells. Cell Stem Cell *18*, 637–652.

Marks, H., Kalkan, T., Menafra, R., Denissov, S., Jones, K., Hofemeister, H., Nichols, J., Kranz, A., Stewart, A.F., Smith, A., et al. (2012). The transcriptional and epigenomic foundations of ground state pluripotency. Cell *149*, 590–604.

Martello, G., and Smith, A. (2014). The nature of embryonic stem cells. Annu. Rev. Cell Dev. Biol. *30*, 647–675.

Martin, G.R. (1981). Isolation of a pluripotent cell line from early mouse embryos cultured in medium conditioned by teratocarcinoma stem cells. Proc. Natl. Acad. Sci. USA *78*, 7634–7638.

Moussaieff, A., Rouleau, M., Kitsberg, D., Cohen, M., Levy, G., Barasch, D., Nemirovski, A., Shen-Orr, S., Laevsky, I., Amit, M., et al. (2015). Glycolysis-mediated changes in acetyl-CoA and histone acetylation control the early differentiation of embryonic stem cells. Cell Metab. *21*, 392–402.

Perry, R.B., and Ulitsky, I. (2016). The functions of long noncoding RNAs in development and stem cells. Development *143*, 3882–3894.

Rosa, A., and Ballarino, M. (2016). Long noncoding RNA regulation of pluripotency. Stem Cells Int. *2016*, 1797692.

Rupaimoole, R., Lee, J., Haemmerle, M., Ling, H., Previs, R.A., Pradeep, S., Wu, S.Y., Ivan, C., Ferracin, M., Dennison, J.B., et al.

(2015). Long noncoding RNA ceruloplasmin promotes cancer growth by altering glycolysis. Cell Reports *13*, 2395–2402.

Sauvageau, M., Goff, L.A., Lodato, S., Bonev, B., Groff, A.F., Gerhardinger, C., Sanchez-Gomez, D.B., Hacisuleyman, E., Li, E., Spence, M., et al. (2013). Multiple knockout mouse models reveal lincRNAs are required for life and brain development. Elife *2*, e01749.

Scarola, M., Comisso, E., Pascolo, R., Chiaradia, R., Marion, R.M., Schneider, C., Blasco, M.A., Schoeftner, S., and Benetti, R. (2015). Epigenetic silencing of Oct4 by a complex containing SUV39H1 and Oct4 pseudogene lncRNA. Nat. Commun. *6*, 7631.

Sheik Mohamed, J., Gaughwin, P.M., Lim, B., Robson, P., and Lipovich, L. (2010). Conserved long noncoding RNAs transcriptionally regulated by Oct4 and Nanog modulate pluripotency in mouse embryonic stem cells. RNA *16*, 324–337.

Sperber, H., Mathieu, J., Wang, Y., Ferreccio, A., Hesson, J., Xu, Z., Fischer, K.A., Devi, A., Detraux, D., Gu, H., et al. (2015). The metabolome regulates the epigenetic landscape during naive-to-primed human embryonic stem cell transition. Nat. Cell Biol. *17*, 1523–1535.

Suckale, J., Wendling, O., Masjkur, J., Jager, M., Munster, C., Anastassiadis, K., Stewart, A.F., and Solimena, M. (2011). PTBP1 is required for embryonic development before gastrulation. PLoS One *6*, e16992.

Takashima, Y., Guo, G., Loos, R., Nichols, J., Ficz, G., Krueger, F., Oxley, D., Santos, F., Clarke, J., Mansfield, W., et al. (2014). Resetting transcription factor control circuitry toward ground-state pluripotency in human. Cell *158*, 1254–1269.

Taleahmad, S., Mirzaei, M., Parker, L.M., Hassani, S.N., Mollamohammadi, S., Sharifi-Zarchi, A., Haynes, P.A., Baharvand, H., and Salekdeh, G.H. (2015). Proteome analysis of ground state pluripotency. Sci. Rep. *5*, 17985.

Tesar, P.J., Chenoweth, J.G., Brook, F.A., Davies, T.J., Evans, E.P., Mack, D.L., Gardner, R.L., and McKay, R.D. (2007). New cell lines from mouse epiblast share defining features with human embryonic stem cells. Nature *448*, 196–199.

Theunissen, T.W., Powell, B.E., Wang, H., Mitalipova, M., Faddah, D.A., Reddy, J., Fan, Z.P., Maetzel, D., Ganz, K., Shi, L., et al. (2014). Systematic identification of culture conditions for induction and maintenance of naive human pluripotency. Cell Stem Cell *15*, 471–487.

Tsai, M.C., Manor, O., Wan, Y., Mosammaparast, N., Wang, J.K., Lan, F., Shi, Y., Segal, E., and Chang, H.Y. (2010). Long noncoding RNA as modular scaffold of histone modification complexes. Science *329*, 689–693.

Wang, Y., Xu, Z., Jiang, J., Xu, C., Kang, J., Xiao, L., Wu, M., Xiong, J., Guo, X., and Liu, H. (2013). Endogenous miRNA sponge lincRNA-RoR regulates Oct4, Nanog, and Sox2 in human embryonic stem cell self-renewal. Dev. Cell *25*, 69–80.

Zhou, W., Choi, M., Margineantu, D., Margaretha, L., Hesson, J., Cavanaugh, C., Blau, C.A., Horwitz, M.S., Hockenbery, D., Ware, C., et al. (2012). HIF1alpha induced switch from bivalent to exclusively glycolytic metabolism during ESC-to-EpiSC/hESC transition. EMBO J. *31*, 2103–2116.